

## Excitation of terahertz radiation by laser pulses in nonuniform plasma channels

Thomas M. Antonsen, Jr. and John Palastro

*Institute for Research in Electronics and Applied Physics, University of Maryland, College Park, Maryland 20742*

Howard M. Milchberg

*Institute for Physical Science and Technology, University of Maryland, College Park, Maryland 20742*

(Received 21 December 2006; accepted 21 February 2007; published online 30 March 2007)

The excitation of terahertz radiation by laser pulses propagating in miniature plasma channels is considered. Generation of radiation by laser pulses in uniform plasmas is generally minimal. However, if one considers propagation in corrugated plasma channels, conditions for radiation generation can be met due to the inhomogeneity of the channel and the presence of guided waves with subluminal phase velocities. It is found that for channels and laser pulses with parameters that can be realized today, energy conversion rates of a fraction of a joule per centimeter can be achieved. Miniature corrugated channels can also be used for creation of THz radiation by bunched electron beams. © 2007 American Institute of Physics. [DOI: 10.1063/1.2715864]

### I. INTRODUCTION

Electromagnetic terahertz radiation spans the range of wavelengths from millimeters to infrared. It has many potential applications in biological imaging, spectroscopy of solids and liquids, and remote sensing.<sup>1</sup> Coherent pulses of THz radiation are especially of interest for time domain spectroscopy.<sup>2</sup> Conventional sources of THz radiation using short pulse lasers rely on pulse generation in a solid and are generally limited to  $\mu\text{J}/\text{pulse}$ .<sup>3</sup> Higher energies per pulse can be generated at accelerator facilities with intense bunched electron beams<sup>4</sup> via synchrotron or transition radiation. Recently, intense THz pulses with energies in the range 10–100  $\mu\text{J}/\text{pulse}$  have been generated as transition radiation by a laser generated and accelerated electron beam passing from plasma to vacuum.<sup>5–7</sup> Here we present a scheme for THz radiation generation that involves the creation of miniature corrugated plasma channels (period  $\sim 40 \mu\text{m}$ ) that act as slow wave structures. THz radiation can be generated in these channels by either the ponderomotive currents driven by a laser pulse (considered in the present paper) or by a beam of electrons accelerated by the laser pulse. Our calculations show that a large fraction of laser pulse energy can be down-converted to THz levels.

Research on THz radiation generation by laser pulses propagating in plasmas has been active since its demonstration by Hamster *et al.*<sup>8</sup> The laser pulse exerts a low-frequency force on plasma electrons leading to a current that has a spectral width that is determined by the temporal duration of the laser pulse and the natural oscillation frequency of the modes supported by the plasma. It is tempting to consider this current density as a source for radiation. However, care must be taken in evaluation of the spatial distribution of the current density.<sup>9</sup> Specifically, the electrostatic or longitudinal part of the current density does not lead to radiation. In addition to having a current density as a source, it is required that the radiation modes of the plasma that couple to the

source have a charge density perturbation. This can be accomplished if the plasma is immersed in a strong magnetic field,<sup>10,11</sup> or if the plasma is inhomogeneous.<sup>8</sup> An alternative approach is for the pulse to excite plasma waves, which normally would be trapped in the plasma, but then by a process of mode conversion, the plasma wave energy is transferred to an electromagnetic (EM) wave.<sup>12</sup> An additional factor that limits the efficiency of conversion of energy from the laser pulse to THz radiation is the lack of phase matching ( $f$ ) or electromagnetic modes. The ponderomotive (PM) current, which is a source for the radiation, travels with the laser pulse at its group velocity, which is below the speed of light. This current density will strongly excite only modes whose phase velocity matches the group velocity of the current source. The radiation modes of the system tend to have phase velocities above the speed of light. Thus, strong excitation is not expected.

In this paper we will investigate a scheme for excitation of THz radiation by the ponderomotive force of a laser pulse that addresses the two main issues previously discussed. The scheme involves the excitation of radiation in a corrugated plasma waveguide. These channels have recently been made in the laboratory, and have been shown to have quite reproducible parameters.<sup>13,14</sup> A schematic diagram of the experimental configuration appears in Fig. 1. A plasma channel is formed by focusing a spatially modulated 500 mJ, 100 ps laser pulse (the formation pulse) through an axicon into a gas jet. This leads to an axially modulated break down along the axis of the axicon and an outward propagating shock wave that is similarly modulated. The period of the modulation is controlled by the spatial modulation of the formation pulse, and can be varied over a wide range of values from 35  $\mu\text{m}$  to several millimeters. A second pulse (100 mJ, 50 fs), delayed by about 2 ns with respect to the formation pulse, is injected into the channel through a hole in the axicon. This pulse will be used to drive currents that generate THz radiation in the channel. This is possible because the electron density is

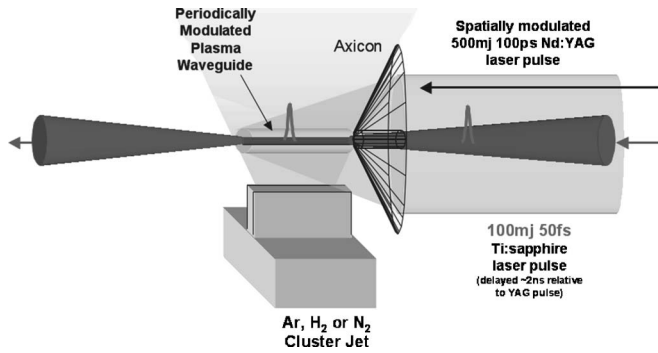


FIG. 1. Schematic diagram of the experimental setup for the generation of axially modulated plasma channels of Ref. 13.

inhomogeneous in the channel. Thus, the radiation modes acquire a density perturbation and can couple to ponderomotively driven currents. Further, the presence of axial corrugations introduces spatial harmonics to the modes that are at multiples of the wavelength corresponding to the period of the corrugations. Thus, the field contains waves that are slower than the speed of light and that can match the velocity of the ponderomotive current.

The organization of the paper is as follows. Section II presents a general calculation for the excitation of THz radiation in periodically corrugated plasma channels. The calculation is similar to that of the excitation of plasma waves, but makes use of the properties of modes of a radially and axially inhomogeneous plasma channel. In Sec. III we introduce a simple model for a periodically corrugated channel that allows for an evaluation of the expressions derived in Sec. II. Using this model we compute the rate of conversion of laser pulse energy to THz levels. We tabulate this rate for an interesting set of parameters and compare the rate of conversion to THz radiation with the rate of conversion to plasma waves. We find a window of parameters where conversion of laser pulse energy to THz radiation is efficient. In Sec. IV we state our conclusions, and we discuss some effects not included in our model that deserve closer study.

## II. EXCITATION OF RADIATION BY A PONDEROMOTIVE POTENTIAL

When an ultrashort, intense laser pulse travels through a uniform plasma, the energy of the pulse is depleted due to the excitation of a plasma wave wake. In a nonuniform plasma channel, an electromagnetic wave wake can be excited as well. We now calculate the rate of energy depletion, due to the excitation of electromagnetic waves with frequency well below that of the laser, that can occur in an inhomogeneous plasma channel. Let us suppose that the laser pulse exerts a force  $\mathbf{F}$  on the plasma electrons, which results in an electron current density  $\mathbf{J}$ . The rate at which the force does work on the current is then given by

$$P_F = \int d^3x \mathbf{F} \cdot \mathbf{J} / q, \quad (1)$$

where  $q = -e$  is the charge of an electron. We now assume that the force is the gradient of a ponderomotive potential,

i.e.,  $\mathbf{F} = -\nabla V_p$ , integrate (1) by parts, and use the continuity equation  $\partial \rho / \partial t = -\nabla \cdot \mathbf{J}$  to express the divergence of the current density. This yields an expression for  $P_F$ ,

$$P_F = - \int d^3x V_p \frac{\partial \tilde{n}}{\partial t}, \quad (2)$$

where  $\tilde{n}$  is the perturbed electron density. Thus, it is clear that the force can only do work on excitations for which there is a perturbed electron density. In the case of a cold, uniform plasma, this implies that work can be done on electrostatic plasma oscillations, which have an electron density perturbation, but not on electromagnetic waves, which have no electron density perturbation. In a nonuniform plasma, or in a magnetized plasma, electromagnetic waves acquire a density perturbation and then the ponderomotive force can do work on them.

Before calculating the rate at which energy is transferred to electromagnetic waves, we repeat the calculation for the rate at which energy is transferred to plasma waves. According to the Poisson equation the divergence of the electric field can be expressed in terms of the perturbed electron density  $\tilde{n}$ ,  $\nabla \cdot \mathbf{E} = 4\pi q \tilde{n}$ . In the limit of a weak ponderomotive potential, the density perturbation satisfies a linear inhomogeneous equation

$$\frac{\partial^2}{\partial t^2} \tilde{n} + \omega_p^2 \tilde{n} = \frac{n_0}{m} \nabla^2 V_p, \quad (3)$$

where the plasma frequency is given by  $\omega_p^2 = 4\pi q^2 n_0 / m$ , and  $n_0$  is the ambient electron density and  $m$  the electron mass. We express the time and space dependence of the ponderomotive potential in terms of an integral,

$$V_p(\mathbf{x}, t) = \int \frac{d\omega}{2\pi} \exp[-i\omega(t - z/u_p)] \bar{V}_p(\mathbf{x}_\perp, \omega), \quad (4)$$

where it is assumed the potential is traveling in the  $z$  direction at a speed  $u_p$  without changing shape. Here, the pulse speed  $u_p$  will be essentially the group velocity of the laser pulse, and consequently will be below the speed of light. We have yet to specify a contour for the integration in Eq. (4). As we will transform Eq. (3) to obtain an expression for the perturbed density, and as we assume that both the perturbed density and its time derivative are zero before the arrival of the pulse, it is appropriate to consider (4) to be a Laplace transform inversion. In this case the integral in Eq. (4) is carried out along a contour parallel to the real  $-\omega$  axis above all the poles of the transform of the perturbed density. In the uniform plasma density case these poles will be at  $\omega = \pm \omega_p$ . Inserting the assumed form of the potential in Eq. (3) and representing the perturbed density in the form of a Laplace integral yields an expression for the transform of the perturbed density that is proportional to the ponderomotive potential. The expression for the rate at which the ponderomotive potential does work on the current can then be written

$$P_{F-PW} = \int \frac{d\omega}{2\pi} \int d^2x_{\perp} \frac{i\omega u_p}{\omega^2 - \omega_p^2} \frac{n_0}{m} \left[ \frac{\omega^2}{u_p^2} \bar{V}_p(\omega) \bar{V}_p(-\omega) + \nabla_{\perp} \bar{V}_p(\omega) \cdot \nabla_{\perp} \bar{V}_p(-\omega) \right]. \quad (5)$$

If the integration contour is pushed down to the real  $-\omega$  axis, then the principal part of the integral is an odd function of  $\omega$  and vanishes. The value of the integral is then determined by the two poles at  $\omega = \pm \omega_p$ ,

$$P_{F-PW} = P_* \frac{u_p}{c} \int d^2x_{\perp} \left[ \frac{\omega_p^2}{u_p^2} \left| \frac{\omega_p \bar{V}_p(\mathbf{x}_{\perp}, \omega_p)}{mc^2} \right|^2 + \left| \nabla_{\perp} \frac{\omega_p \bar{V}_p(\mathbf{x}_{\perp}, \omega_p)}{mc^2} \right|^2 \right], \quad (6)$$

where  $P_* = c(mc^2/q)^2/(8\pi)$  and corresponds to  $3.45 \times 10^8$  W when converted to SI units. The integral in Eq. (6) is a dimensionless quantity that is proportional to the square of the ponderomotive potential measured in units of the electron rest energy. Recall that the overbar on the potential indicates that it is the Laplace transform of the time dependent potential. If we estimate the integral as being of order unity, then it takes 80 cm of propagation to generate 1 J of plasma waves; viz.,  $P_*/c$  corresponds to  $1.16 \times 10^{-2}$  J/cm.

We now evaluate the power transfer in the case in which an electromagnetic mode of the guiding channel is excited by the ponderomotive potential. The channel is assumed to be periodic in axial distance with a period  $d=2\pi/k_0$ . The electric and magnetic fields of the eigenmodes of the channel are characterized by the dimensionless functions  $\mathbf{e}(\mathbf{x}, \omega)$  and  $\mathbf{b}(\mathbf{x}, \omega)$ , which are periodic in  $z$  with the same period as the channel, and which according to Floquet theory satisfy Maxwell's equations,

$$i\omega \mathbf{b} = c(\nabla + ik_c \hat{\mathbf{z}}) \times \mathbf{e}, \quad (7a)$$

and

$$-i\omega \varepsilon \mathbf{e} = c(\nabla + ik_c \hat{\mathbf{z}}) \times \mathbf{b}. \quad (7b)$$

Here,  $\varepsilon(\mathbf{x})$  is the periodic dielectric constant of the plasma that determines the modes of the structure, and  $k_c(\omega)$  is the Floquet wave number associated with frequency  $\omega$ . We assume that the ponderomotive force is weak and resonantly excites the mode. In this case the electric field of the guided mode will be written as a Laplace integral of a frequency-dependent amplitude  $\bar{E}(\omega)$ , multiplying the vector eigenmode  $\mathbf{e}(\mathbf{x}, \omega)$

$$\mathbf{E}(\mathbf{x}, t) = \int \frac{d\omega}{2\pi} \bar{E}(\omega) \mathbf{e}(\mathbf{x}, \omega) \exp[-i\omega(t - z/u_p)], \quad (8)$$

The ponderomotive force drives a current  $\mathbf{J}_F$ , which in turn excites the modes of the channel. The field amplitude can be calculated perturbatively by inserting (8) into Maxwell's equations and projecting on to the eigenfunctions  $\mathbf{e}$  and  $\mathbf{b}$ . The result is

$$\left( \frac{\omega}{u_p} - k_c(\omega) \right) \bar{E}(\omega) = \frac{2\pi i}{cA(\omega)} \int d^2x_{\perp} \langle \mathbf{e}^* \cdot \bar{\mathbf{J}}_F \rangle, \quad (9)$$

where  $\bar{\mathbf{J}}_F$  is the transformed amplitude of the current driven by the ponderomotive force and the angle brackets indicate an average over one period of the channel. The quantity  $A(\omega)$  represents the effective cross-sectional area of the mode, based on power density, i.e.,  $A(\omega) = \int d^2x_{\perp} \text{Re}[\mathbf{e}^* \times \mathbf{b} \cdot \hat{\mathbf{z}}]$ . The transform of the perturbed current can be expressed in terms of the ponderomotive potential and the dielectric constant of the channel:

$$\bar{\mathbf{J}}_F(\mathbf{x}, \omega) = \frac{i\omega}{4\pi q} (\varepsilon - 1) \left( \nabla_{\perp} + i\hat{\mathbf{z}} \frac{\omega}{u_p} \right) \bar{V}_p. \quad (10)$$

Inserting the expression for the current [Eq. (10)] into Eq. (9) allows one to find the amplitude of the electric field:

$$\bar{E}(\omega) = - \frac{u_p \omega \bar{V}_p(\omega)}{2c q A(\omega) (\omega - k_c u_p)}, \quad (11)$$

where

$$\bar{V}_p(\omega) = \int d^2x_{\perp} \bar{V}_p \left\langle \left( \nabla_{\perp} - i\hat{\mathbf{z}} \frac{\omega}{u_p} \right) \cdot \mathbf{e}^* \right\rangle, \quad (12)$$

and the angular brackets indicate an average over one period of the structure. The quantity  $\bar{V}_p(\omega)$  represents the overlap of the ponderomotive potential with the density perturbation (proportional to the divergence of the electric field) associated with the mode of the corrugated channel. Expressing the perturbed density in Eq. (2) in terms of the divergence of the electric field, using Eq. (8) for the electric field, we can calculate the power transfer from the ponderomotive force to the waveguide mode. The power transfer results in an expression that varies periodically in time as the laser pulse moves through the periodic structure. If we average this expression over one period of the oscillation, we obtain

$$P_{F-EM} = \frac{i u_p}{4\pi q} \int \frac{d\omega}{2\pi} \omega \bar{E}(\omega) \bar{V}(-\omega). \quad (13)$$

Substituting the expression for the electric field amplitude obtained from (9) into (13) gives an expression analogous to (5) in the plasma wave case:

$$P_{F-EM} = -i \int \frac{d\omega u_p^2}{16\pi^2 q^2 c A(\omega) (\omega - k_c u_p)} |\omega \bar{V}_p(\omega)|^2. \quad (14)$$

The value of the integral is determined by the contribution of the pole and corresponds to the frequency for which the wave matching condition is satisfied, i.e.,  $\omega = k_c(\omega) u_p$ :

$$P_{F-EM} = P_* \frac{u_p^2/c^2}{(1 - u_p/u_g) A(\omega)} \left| \frac{\omega \bar{V}_p(\omega)}{mc^2} \right|^2, \quad (15)$$

where  $u_g = d\omega/dk_c$  is the group velocity of the waveguide mode, and we have doubled the contribution to account for the poles at positive and negative frequency. We note that the expression here for the transfer of power to radiation has essentially the same form as Eq. (6) for power transferred to plasma waves. Here, however, the ponderomotive potential is weighted by the divergence of the electric field basis vec-

tor before spatial integration. Thus, power will not be transferred to electromagnetic waves that do not have an electron density perturbation. Comparison of these two expressions will be made once we have introduced a simple model that allows us to calculate the modes of a periodic waveguide plasma waveguide.

### III. RADIALLY POLARIZED WAVES IN A CORRUGATED CHANNEL

In this section we will introduce and solve a simple model for a periodically corrugated plasma channel. This will determine the modes described by Eqs. (7a) and (7b) and allow for the rough evaluation of the integrals in Eq. (12) that will lead to an estimation of the power transfer to electromagnetic waves according to (15). The model that we consider is that of a plasma channel for which the electron density near the axis varies in both radius and axial coordinate:

$$n_0(r, z) = n_{00} \left[ 1 + \frac{r^2}{2r_{\text{ch}}^2} + \Delta \sum_{l=-\infty}^{\infty} \delta(z - ld) \right]. \quad (16)$$

That is, the channel has a parabolic profile in radius and a sequence of delta-function peaks, with period  $d$  and strength  $\Delta$ , in axial distance. We consider radially polarized, azimuthally symmetric, transverse magnetic modes ( $e_r, b_\theta, e_z$ ) with  $e_r \gg e_z$  for which the approximate mode equation can be written:

$$\frac{\partial}{\partial r} \frac{\partial}{\partial r} r e_r + \frac{\partial^2}{\partial z^2} e_r + \frac{\omega^2}{c^2} e_r = \frac{\omega_p^2(r, z)}{c^2} e_r. \quad (17)$$

We now assume that the radial dependence of the radial electric field corresponds to the lowest mode of the uniform sections of the channel,

$$e_r(r, z) = e_\perp(z) (r/w) \exp(-r^2/w^2), \quad (18)$$

where  $8w^{-4} = \omega_{p0}^2 / (c^2 r_{\text{ch}}^2)$  defines the radial mode width  $w$ , and  $\omega_{p0}^2 = 4\pi q^2 n_{00} / m$  is the plasma frequency at the channel axis. This results in an ordinary differential equation for the  $z$ -dependent amplitude

$$\left( \frac{d^2}{dz^2} + \frac{\omega^2 - \omega_c^2}{c^2} \right) e_\perp(z) = \frac{\omega_{p0}^2}{c^2} \Delta \sum_{l=-\infty}^{\infty} \delta(z - ld) e_\perp(z), \quad (19)$$

where  $\omega_c^2 = \omega_{p0}^2 + 8c^2/w^2$  is the cutoff frequency for the lowest mode in the uniform sections of the channel.

We now solve Eq. (19) subject to the Floquet condition, i.e.,  $e_\perp(z+d) = e_\perp(z) e^{ik_c(\omega)d}$ , where  $k_c(\omega)d$  is the phase advance per period of the solution, and  $k_c$  is the Floquet wave number introduced in Eqs. (7a) and (7b). In the axially uniform regions the solutions have the form of forward and backward going waves, i.e.,

$$e_\perp(z) = e_+^{><} \exp(ik_f z) + e_-^{><} \exp(-ik_f z), \quad (20)$$

where  $k_f = \sqrt{(\omega^2 - \omega_c^2)/c^2}$  is the axial wavenumber in the uniform portion of the channel, and the “>” and “<” signs correspond to  $d > z > 0$  and  $-d < z < 0$ , respectively. Relations between the amplitudes of the forward and backward waves on either side of  $z=0$  are obtained from the boundary

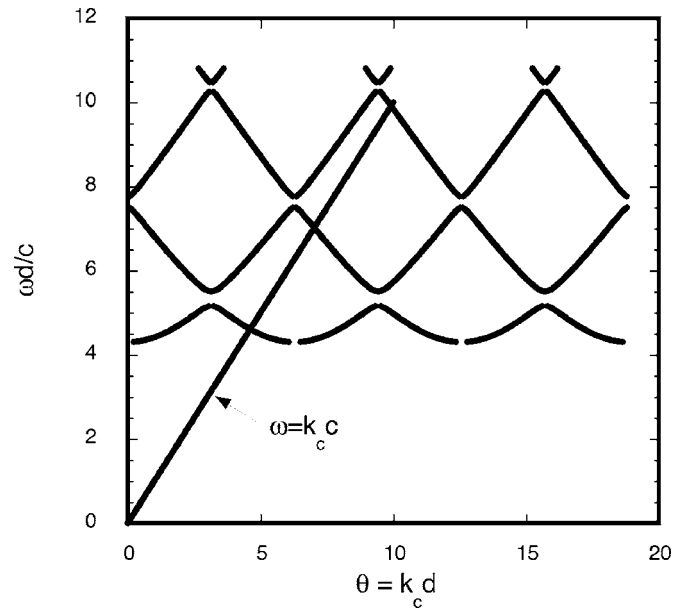


FIG. 2. Dispersion curves,  $\omega$  vs  $k_c$ , for a periodically modulated channel with normalized modulation size  $R = \omega_{p0}^2 d \Delta / (2c^2) = 1$  and  $\omega_c d / c = 1.41$ , according to Eq. (21). Here,  $d$  is the period of the channel.

conditions corresponding to the continuity of  $e_\perp$ , and the jump condition obtained by integrating Eq. (20) across the delta-function at  $z=0$ ,  $de_\perp/dz|_{0^+} = (\omega_{p0}^2 \Delta / c^2) e_\perp(0)$ . Finally, application of the Floquet condition, i.e.,  $e_\pm^{<} = e_\pm^{>} \exp(\pm ik_f d + ik_c d)$  results in a dispersion relation for  $k_c(\omega)$ ,

$$\cos(k_c d) = \cos(k_f d) + \frac{R}{k_f d} \sin(k_f d), \quad (21)$$

where  $R = \omega_{p0}^2 d \Delta / (2c^2)$  measures the strength of the periodic modulations of the channel. In addition, as a by-product of the preceding conditions, we obtain a relation between the amplitude of the forward and backward waves:

$$\frac{e_-^{><}}{e_+^{><}} = - \frac{1 - \exp[i(k_f - k_c)d]}{1 - \exp[-i(k_f + k_c)d]}. \quad (22)$$

Equation (21) can be interpreted as follows. For a given value of frequency  $\omega$  (and consequently, a given value of  $k_f$ ), values of the Floquet wavenumber  $k_c$  are determined. Note that if  $k_c$  is a value that satisfies Eq. (21), then so do  $k_c + 2\pi n/d$  and  $2\pi m/d - k_c$ , where  $m$  and  $n$  are integers. Therefore, frequency will be an even periodic function of  $k_c d$ . Note also, that since  $|\cos(k_c d)| \leq 1$  for real  $k_c$ , there will be intervals of frequency and  $k_f$  values for which Eq. (21) has no solutions. These intervals correspond to stop bands that appear in the presence of axial corrugations of the channel. Note also that in the case of no corrugations, i.e.,  $R=0$ ,  $k_c = \pm k_f$ , and according to Eq. (22) the solutions are either purely forward or purely backward propagating waves, as expected.

A plot of  $\omega d/c$  versus  $k_c d$  for the case of  $R=1$  and  $\omega_c d/c = 1.41$  appears in Fig. 2. The periodic dependence of  $\omega$ , and on  $k_c$  is evident, as are the stop bands. Also shown in this plot is a straight line (the light line)  $\omega = k_c c$  corresponding to the case of a ponderomotive pulse traveling at the

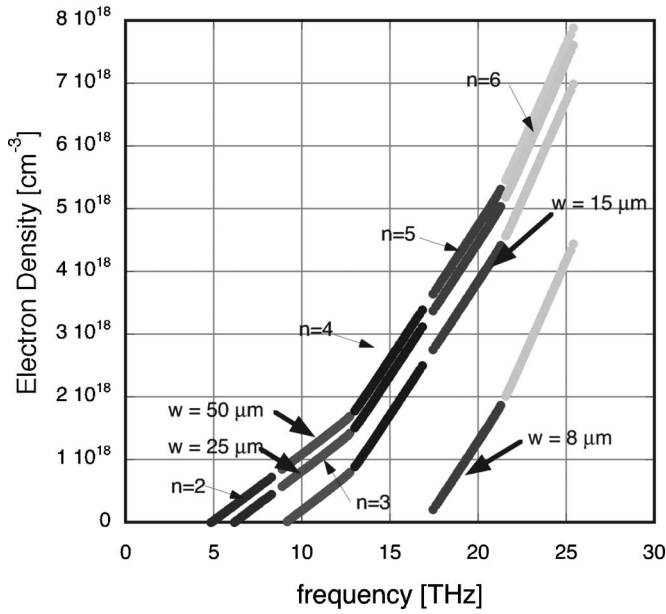


FIG. 3. Electron density vs frequency for channels with period  $d=35 \mu\text{m}$  and various channel widths. The index  $n$ , where  $(n-1)\pi < k_c d < n\pi$ , gives the range of  $k_c$  values for which the light line and dispersion curves cross.

speed of light. The intersection of this line and the dispersion curves define (s) the frequency for which wave phase matching occurs and corresponds to the pole in Eq. (14). We note that in the case of Fig. 2 the lowest-frequency intersection occurs for  $\pi < k_c d < 2\pi$  and that in this range of wavenumbers the waveguide mode is a backward wave. Thus, the radiated power in this case will propagate counter to the direction of the laser pulse.

For given values of the central plasma frequency  $\omega_{p0}^2$ , radial mode width  $w$ , and corrugation period  $d$ , we can find the intersection point between the dispersion curve and the light line (assuming the laser pulse is propagating near the speed of light) and determine the operating frequency. Results of such a calculation are plotted in Fig. 3 in the form of electron density versus frequency for a structure with period  $d=35 \mu\text{m}$  and several values of the radial mode width  $w$ . The intersections occur in different ranges of  $k_c d$  depending on parameters. The ranges are indicated by the integer  $n$ , where  $(n-1)\pi < k_c d < n\pi$ . The lowest-frequency intersection of Fig. 2 is classified as being  $n=2$  in this scheme. Even (odd) values of  $n$  thus correspond to backward (forward) wave intersections.

The present model can be used to evaluate the coupling coefficient (12) in addition to determining the dispersion relation as just described. In particular,

$$\langle (\nabla_{\perp} + i\hat{z}k_c) \cdot \mathbf{e} \rangle = \int_0^d \frac{dz}{d} e^{-ik_c z} \left[ \frac{\partial}{\partial r} (r e_r) + i k_c e_z \right], \quad (23)$$

where we have evaluated the coefficient for  $\omega = k_c u_p$  corresponding to the pole in (14).

The axial electric field of the TM mode can be found in the uniform sections of the channel to be given by

$$e_z(r, z > 0) = \frac{2i}{k_f w} \left( 1 - \frac{r^2}{w^2} \right) \exp\left(-\frac{r^2}{w^2}\right) (e_+^> \exp(ik_f z) - e_-^> \exp(-ik_f z)). \quad (24)$$

Thus we have, carrying out the integral in (23),

$$\langle (\nabla_{\perp} + i\hat{z}k_c) \cdot \mathbf{e} \rangle = \frac{4}{w} \left( 1 - \frac{r^2}{w^2} \right) e^{i[-r^2/w^2 + i(k_f - k_c)d/2]} e_+^> \times \frac{\sin[(k_f - k_c)d/2]}{k_f d/2}, \quad (25)$$

where we have used the ratio of backward to forward waves (22) to eliminate the backward wave amplitudes in  $e_r$  and  $e_z$ . Expression (25) is relatively simple; however, it should be used with caution. Note that the value of the coupling coefficient exhibits essentially no dependence on which range  $n$  of values  $[(n-1)\pi < k_c d < n\pi]$   $k_c d$  is considered to lie in. This is because of the delta-function nature of our axial density profile. In our model the electric field has zero divergence in the uniform sections of the channel and possibly infinite divergence at the location of each delta-function peak in the channel density. Thus, the integral in (23) will have an oscillatory dependence on the value of  $k_c$ . In a more realistic model, the high-density regions will have a nonzero thickness, and the value of the integral will tend to zero for  $k_c$  values that are greater than the inverse of this thickness. As a result, the coupling to modes with larger values of the index  $n$  in Fig. 3 will be smaller than the coupling to the lowest values of  $n$ . We therefore expect the electromagnetic wave generation to be more efficient for the lower values of  $n$ . Quantification of this effect requires a more realistic model of the channel density profile, and will be left to future work. For the time being we will assume that (25) is accurate for low values of  $n$  and proceed.

The effective area of the mode,  $A(\omega) = \int d^2 x_{\perp} \text{Re}[\mathbf{e}^* \times \mathbf{b} \cdot \hat{z}]$ , can be calculated using the given radial profile of the mode (20) along with the relation

$$b_{\theta}(r, z > 0) = \frac{\omega}{k_f c} \left( 1 - \frac{\omega_{p0}^2}{\omega^2} \right) \frac{r}{w} \exp\left(-\frac{r^2}{w^2}\right) (e_+^> \exp(ik_f z) - e_-^> \exp(-ik_f z)).$$

We find that

$$A(\omega) = \frac{\pi w^2 \omega}{4 k_f c} \left( 1 - \frac{\omega_{p0}^2}{\omega^2} \right) |e_+^>|^2 \left[ 1 - \frac{\sin^2[(k_f - k_c)d/2]}{\sin^2[(k_f + k_c)d/2]} \right].$$

We now take the ponderomotive potential to have the form

$$V_p(\mathbf{x}, t) = V_{p0} f(t - z/u_p) \exp(-2r^2/r_{sp}^2), \quad (26)$$

where the function  $f(t)$  gives the temporal profile of the pulse and  $r_{sp}$  is the spot-size of the laser pulse. If the laser pulse is a guided mode of the channel, then  $r_{sp} = w$ . We Fourier transform the ponderomotive potential in time, multiply by the divergence of the electromagnetic field of the mode given by (25) and integrate over radius according to (12) to obtain

$$\bar{V}_p = \bar{f}(\omega) V_{p0} e^{i(k_f - k_c)d/2} e^{>} \frac{8\pi w^3 r_{sp}^2 \sin[(k_f - k_c)d/2]}{(r_{sp}^2 + 2w^2)^2 k_f d/2}, \quad (27)$$

where  $\bar{f}(\omega)$  is the Fourier transform of the pulse shape. Combining the above factors, we arrive at the following expression for the rate of power transfer to electromagnetic radiation,

$$P_{F-EM} = P_* F_1 F_2 \left| \frac{\omega \bar{f}(\omega) V_{p0}}{mc^2} \right|^2, \quad (28)$$

where

$$F_1 = \pi \frac{(4r_{sp}w)^4}{(r_{sp}^2 + 2w^2)^4}, \quad (29)$$

and

$$F_2 = \frac{\omega^2}{(\omega^2 - \omega_{p0}^2)} \frac{u_p}{(u_p - u_g)} \left( \frac{k_f d}{\omega} \right) \frac{R^2 \sin(k_f d)}{(k_f d)^4 \sin(k_c d)}. \quad (30)$$

The group velocity is obtained by differentiation of the dispersion relation with respect to frequency:

$$\frac{u_g}{c} = \frac{k_f c}{\omega} \left\{ \frac{(k_f d)^2 \sin(k_c d)}{[R + (k_f d)^2] \sin(k_f d) - k_f d R \cos(k_f d)} \right\}. \quad (31)$$

The power transfer to electromagnetic waves is the product of a fixed power  $P_*(3.45 \times 10^8 \text{ W})$  and three dimensionless quantities. Under the same assumptions on the ponderomotive potential (26) we can evaluate the power transfer to plasma waves (6),

$$P_{F-PM} = P_* \frac{\pi}{4} \left[ 1 + \frac{\omega_{p0}^2 w^2}{c^2} \right] \left| \frac{\omega_p \bar{f}(\omega_p) V_{p0}}{mc^2} \right|^2, \quad (32)$$

which is to be compared with Eq. (28).

In the expression for generation of electromagnetic radiation, factor  $F_1$  accounts for the overlap of the radiation pulse with the electromagnetic mode of the waveguide. This factor has a peak value of  $4\pi = 12.57$  when  $r_{sp}^2 = 2w^2$ . However, the maximum is broad, being above 9.9 for  $w^2 < r_{sp}^2 < 4w^2$ . Factor  $F_2$  can be evaluated once the parameters of the channel are specified. Such an evaluation has been made for the case  $R=1$ ,  $d=50 \mu\text{m}$ , and several values of mode width  $w$ . Results are plotted in Fig. 4, where coupling coefficient  $F_2$  and electron density are plotted versus generated frequency. We note that the coupling strength generally increases with frequency, while exhibiting large variations. The general increase is due mainly to the first factor in Eq. (30). With fixed channel dimensions, increasing frequency requires increasing plasma density and as a result, the relative difference between the wave and plasma frequencies decreases. There is also a set of frequencies for which the coupling factor vanishes. These frequencies correspond to cases in which the intersection in Fig. 2 occurs at a so-called “ $\pi$ ”-point in the dispersion curve; that is, when  $k_c d = m\pi$ , where  $m$  is an odd integer. At these points both  $k_c d$  and  $k_f d$  equal an odd integer multiple of  $\pi$  and the last term in Eq. (27) vanishes. Physically, for  $\pi$ -point modes, the radial electric field has the opposite sign in adjacent cells of the struc-

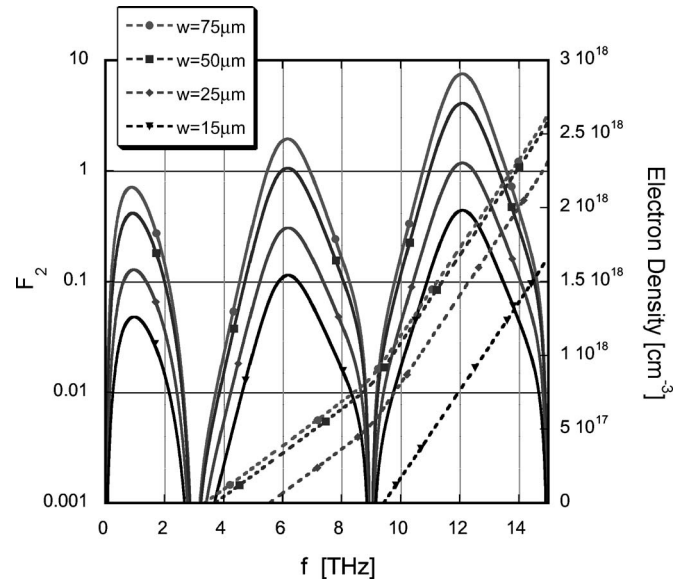


FIG. 4. Coupling coefficient and electron density vs frequency for channels with period  $d=50 \mu\text{m}$ , various channel widths and  $R=1$ . Coupling minima occur for  $k_c d = m\pi$ , where  $m$  is an odd integer.

ture and vanishes at the location of the high-density (delta-function) regions. The vanishing of the radial field at these points implies that the axial field does not vary at the location of the high-density region. The divergence of the electric field thus vanishes at the location of the delta-functions and the coupling is zero. The coupling maximizes at the  $2\pi$ -points. Here, the radial field has the same direction in each cell, and the direction of the axial field reverses at the location of the delta-functions. This implies a relatively large electric field divergence and associated with that, a large density perturbation. If we consider a  $w=50 \mu\text{m}$  wide mode at 6 THz, we then arrive at a value of the product  $F_1 F_2 \cong 10$ .

In general, the conditions required to excite a  $2\pi$ -mode at a particular frequency can be obtained as follows. Equation (21) with  $k_c d = 2\pi m$ , determines the normalized cutoff wavenumber  $k_f d$  for different values of  $R$ , which characterizes the size of the modulations. For example, with  $R=1$ , the normalized cutoff wavenumber is  $k_f d = 1.31$ . Using the definition of  $k_f$  following (20) and  $\omega_c$  following (19), we have

$$\omega = \sqrt{\omega_{p0}^2 + c^2(8/w^2 + 1.72/d^2)} = 2\pi m c d, \quad (33)$$

where the second equality follows from the requirement that the dispersion curve intersect the light line with  $k_c d = 2\pi m$ . Thus, if a particular frequency is desired for an  $m=1$  spatial harmonic interaction, one must pick the period  $d$  of the modulations based on the second equality in (33), and then channel density  $\omega_{p0}^2$  and radial mode width  $w$ , to satisfy the first equality in (33). On the other hand, if two of the parameters of density, mode width, and period are specified, the second equality in (33) determines the third, and the first the frequency.

The remaining factor that controls the rate of generation of radiation is the amplitude of the normalized ponderomotive potential. For a given pulse power this quantity will

TABLE I. Depletion rate for modes with various widths for a 1 J laser pulse and  $d=50 \mu\text{m}$ .

$w$ [ $\mu\text{m}$ ]	$V_{p0}/mc^2$	$F_2$	$f$ [THz]	$dU/dz$ [J/cm]	$n_e$ [ $\text{cm}^{-3}$ ]
75	0.040 050	1.94	6	$8.339\ 64 \times 10^{-4}$	$3.9381 \times 10^{+17}$
50	0.090 112	1.06	6	$2.306\ 83 \times 10^{-3}$	$3.4359 \times 10^{+17}$
25	0.36045	0.31	6	$1.062\ 01 \times 10^{-2}$	$7.2387 \times 10^{+16}$
15	—	—	6	—	—
75	0.080 100	7.54	12	$1.296\ 51 \times 10^{-2}$	$1.7393 \times 10^{+18}$
50	0.180 22	4.09	12	$3.560\ 36 \times 10^{-2}$	$1.6891 \times 10^{+18}$
25	0.720 90	1.18	12	$1.643\ 51 \times 10^{-1}$	$1.4179 \times 10^{+18}$
15	2.0025	0.44	12	$4.728\ 66 \times 10^{-1}$	$7.7503 \times 10^{+17}$

scale as the negative fourth power of the radius  $w$  assuming the spotsize and radius are fixed. In particular,

$$\frac{V_{p0}}{mc^2} = \frac{\lambda^2}{4\pi^{7/2}r_s^2 t_D P_*} U_L = 1.32 \times 10^4 \frac{\lambda^2 U_L [\text{J}]}{r_s^2 t_D [\text{fs}]},$$

where  $\lambda$  is the wavelength of the laser radiation,  $U_L$  is the pulse energy, and  $t_D$  is the half-width at  $e^{-1}$  of the laser intensity. For a Gaussian temporal profile of the laser pulse the Fourier transform of the ponderomotive potential is given by  $\omega \bar{f}(\omega) = \pi^{1/2} \omega t_D \exp[-(\omega t_D)^2/4]$ , which has a peak value of 1.52 when  $\omega t_D = \sqrt{2}$ . For 6 THz radiation, the optimum value of  $t_D$  is 37.5 fs. We thus arrive at the depletion rates listed in Table I. For a 1 J,  $0.8 \mu\text{m}$  laser pulse with time duration  $t_D = 37.5$  fs, for 6 THz and  $t_D = 18.8$  fs for 12 THz.

The corresponding electron densities for the entries in Table I are obtained from Fig. 4. The highest depletion rate is obtained for a channel with a  $15 \mu\text{m}$  mode width at a density just below  $10^{18} \text{cm}^{-3}$ . The generated frequency in this case is 12 THz.

An important consideration is a comparison between the rate of generation of radiation and plasma waves: the ratio of Eqs. (28)–(32). This quantity is plotted in Fig. 5 as a function of frequency. The ratio has peaks at the frequencies corresponding to local maxima of the coupling coefficient  $F_2$  as expected. It also has a peak towards lower frequencies due to the fact that the central channel density is tending toward zero and the excitation of plasma waves becomes small. Frequencies below the point where the ratio diverges should be disregarded as they correspond to negative central electron densities. Figure 5 shows that to maximize the fraction of energy transferred to THz radiation, one is lead to consider more narrow channels, even though coupling to modes to larger channels appears to be stronger. For example, for  $15 \mu\text{m}$  channels with density  $7.8 \times 10^{17}$ , roughly twice as much energy is transferred to radiation as is to plasma waves.

#### IV. DISCUSSION

In order for the present scheme to be a useful source of THz radiation, the power that is transferred from the laser pulse to the waveguide mode, calculated in the preceding sections, must be able to escape the plasma. A number of factors may limit this process. First, the waveguide mode

may suffer either collisional or collisionless damping. Further, the modes of the plasma channel have to couple to free space radiation at the plasma boundary.

The importance of collisional damping can be assessed by evaluation of the product of the wave frequency and the electron collision time  $\tau_e \omega$ . The electron collision time is sensitive to the electron temperature. For channels formed by hydrodynamic expansion,<sup>15</sup> the electron temperature is in the range  $T_e$ ; i.e., 100 eV. Thus, if we consider the last entry in Table I, we find  $\tau_e \omega = 2.25 \times 10^3$ . Thus, one could expect the THz radiation damping length due to collisions to correspond to a large number of periods of the structure, and the amount of extracted energy could be as high as the product of the extraction rate and this length. A more accurate assessment of the damping length including the effects of the THz radiation group velocity awaits a more realistic model of the plasma channel.

Collisionless damping may place a more severe restriction on the interaction length. In the uniform sections of the

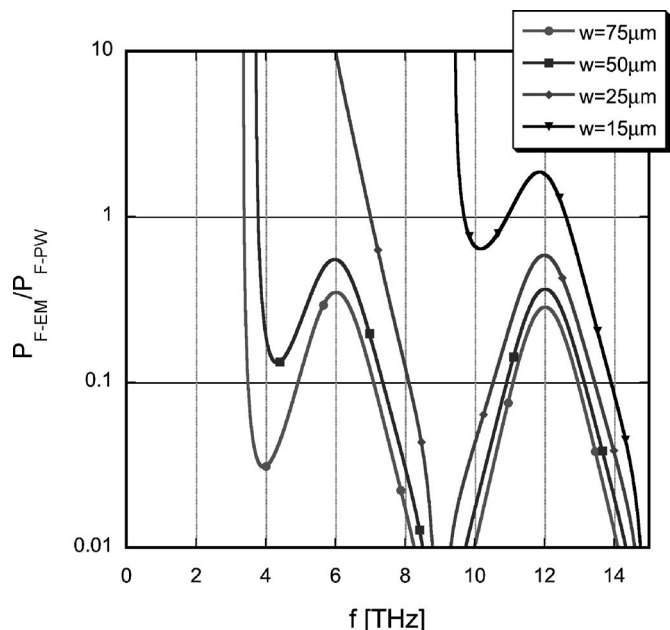


FIG. 5. The ratio of power transferred to THz radiation to power transferred to plasma waves for laser pulses in channels with period  $d=50 \text{mm}$ ,  $R=1$ , and various channel widths. The ratio peaks for modes that satisfy  $k_c d = m\pi$ , where  $m$  is an even integer.

channel in the model discussed in Sec. IV, the mode is confined by the parabolic variation of the electron density. The mode width is determined by the location of the turning point  $r_t$ , where  $\omega_p^2(r_t) = \omega^2 - k_f^2 c^2 = \omega_p^2(0) + 8c^2/w^2$ . At a larger radius  $r_s$ , where  $\omega_p^2(r_s) = \omega^2$ , the mode frequency is resonant with the local plasma frequency, and collisionless absorption can be expected. The damping will be small if the mode amplitude is small at the radius  $r_s$ . This requires, in the case of a parabolic channel, that  $r_s^2/w^2 = 2 + (k_f w)^2/4$  be large. If we estimate the damping to scale as the mode amplitude at the resonant surface, and estimate the mode to have a Gaussian dependence on radius, we then find  $\exp(-r_s^2/w^2) = 0.130\ 21, 0.121\ 57, 0.088\ 123, 0.051\ 545$ , respectively, for modes of width  $w = 15, 25, 50$ , and  $75\ \mu\text{m}$  for the 12 THz entries in Table I. Thus, for parabolic channels, damping will be small only if the channel width is large enough. One could imagine circumventing this problem by considering leaky channels,<sup>16</sup> which have a peak electron density below the critical density for the generated radiation. In these channels radiation will be lost to leakage through the walls. If the wall is thick, this rate of loss can be made exponentially small.

Once energy has been deposited in the form of a THz mode in the channel, a way must be found to extract that energy for the desired applications. Two possibilities present themselves: end coupling and side coupling. For end coupling, we can imagine that the properties of the corrugated channel (for example, the strength of the periodic modulation) can be slowly varied with axial distance. In terms of the dispersion curves pictured in Fig. 2, we can imagine that with axial distance the modulation amplitude decreases and the stop bands close, leaving a uniform waveguide dispersion relation. In this case, the generated wave will smoothly transform to a superluminal mode of a smooth waveguide, which then will be easily transmitted through the boundary at the end of the channel. The direction of the radiated energy will depend on the sign of the group velocity at the point of intersection of the dispersion curve and pulse line  $\omega = k_c u_p$ . For example, the case depicted in Fig. 2 involves a backward wave. Gradual variation in space of parameters of the channel also offers the possibility to engineer the properties of the THz pulse. For example, variation of the period will give rise to a chirped THz pulse. Such pulses may be further compressed by transmitting them through a medium with a known dispersion. A possible drawback to end coupling is the issue of losses mentioned above. In this case, side coupling may be considered.<sup>15</sup> Side coupling can be understood from the square of the local radial wavenumber; i.e.,  $k_\perp^2 = \omega^2 - \omega_p^2(r) - k_c^2 c^2$ . In the center of the channel this number is positive. It becomes negative in the wall of the channel and then positive again outside the channel. Thus, energy can tunnel through the wall and escape laterally if the wall is not too dense. This phenomenon has already been exploited experimentally for smooth channels.<sup>15</sup> Side coupling is available for our slow wave modes because, in fact, the mode consists of a superposition of partial waves with different spatial wavenumbers. Some of these partial waves will be superluminal and can propagate laterally away from the channel.

The theory outlined so far for THz radiation generation

has assumed that the driving laser pulse shape (or electron beam shape) does not change as energy is depleted from the pulse and converted to THz radiation. Of course, the pulse must evolve as energy is depleted from it. However, we note that preliminary calculations show that a long laser pulse is modulationally unstable to the generation of THz radiation in corrugated channels in analogy to forward Raman scattering that occurs in uniform plasmas. Thus, one can envisage a self-modulated regime in which the envelope of the laser acquires time dependence that enhances the excitation of THz radiation. This represents a three-wave decay scenario in which an electromagnetic wave decays to two lower-frequency electromagnetic waves. This is a process that cannot occur in a uniform plasma, which makes it interesting in its own right.

Finally, a bunched electron beam can also be used to generate THz radiation.<sup>5,6</sup> We can repeat the above analysis, starting with Eq. (9) and consider that  $\mathbf{J}$  is the transform of the beam current density. We arrive at an expression for the power extracted from the beam,

$$P_{\text{Beam}} = \frac{2\pi u_p^2 u_g}{(1 - u_g/u_p) c A} \left| \int d^2 x_\perp \langle \mathbf{e}^* \cdot \bar{\mathbf{J}} \rangle \right|^2 = \frac{1}{2} Z \left| \int d^2 x_\perp \frac{\omega \langle \mathbf{e}^* \cdot \bar{\mathbf{J}} \rangle}{\langle \mathbf{e}^*(0) \cdot \hat{\mathbf{z}} \rangle} \right|^2, \quad (34)$$

where the first equality is expressed in esu, while the second is in SI units. The quantity

$$Z = \frac{u_g}{(u_p - u_g)} \frac{|\langle \mathbf{e}(0) \cdot \hat{\mathbf{z}} \rangle|^2}{k_c^2 \int d^2 x_\perp \text{Re}(\hat{\mathbf{z}} \cdot \mathbf{e}^* \times \mathbf{h})} \quad (35)$$

represents the impedance of the structure. (Recall,  $\bar{\mathbf{J}}$  is the Fourier transform of the current density; thus, the second quantity under the magnitude sign is roughly the peak beam current.) The impedance characterizes the strength of the axial electric field for a given level of power flowing along the structure and is useful in analyzing the effectiveness of the structure for particle acceleration and radiation generation. Future publications will focus on this quantity.

## ACKNOWLEDGMENTS

This work was supported by the US Department of Energy and the National Science Foundation.

<sup>1</sup>D. M. Mittleman, R. H. Jacobsen, and M. C. Nuss, *IEEE J. Sel. Top. Quantum Electron.* **2**, 679 (1996).

<sup>2</sup>M. C. Nuss and J. Orenstein, in *Millimeter-Wave Spectroscopy of Solids*, edited by G. Gruener (Springer-Verlag, Heidelberg, 1997), and references therein.

<sup>3</sup>E. Budiarto, J. Margolies, S. Jeong, J. Son, and J. Bokor, *IEEE J. Quantum Electron.* **32**, 1839 (1996).

<sup>4</sup>T. Nakazato, M. Oyamada, N. Nimura *et al.*, *Phys. Rev. Lett.* **63**, 1245 (1989); U. Happek, A. J. Sievers, and E. Blum, *Phys. Rev. Lett.* **67**, 2962 (1991); M. L. Ter-Mikaelian, *High-Energy Electromagnetic Processes in Condensed Media* (Wiley-Interscience, New York, 1972).

<sup>5</sup>W. P. Leemans, C. G. R. Geddes, J. Faure *et al.*, *Phys. Rev. Lett.* **91**, 074802 (2003).

- <sup>6</sup>W. P. Leemans, J. van Tilborg, J. Faure, C. G. R. Geddes, C. Toth, C. B. Schroeder, E. Esarey, and G. Fubiani, *Phys. Plasmas* **11**, 2899 (2004).
- <sup>7</sup>W. P. Leemans, E. Esarey, J. van Tilborg, P. A. Michel, C. B. Schroeder, C. Toth, C. G. R. Geddes, and B. Shadwick, *IEEE Trans. Plasma Sci.* **33**, 8 (2005).
- <sup>8</sup>H. Hamster, A. Sullivan, S. Gordon, W. White, and R. W. Falcone, *Phys. Rev. Lett.* **71**, 2725 (1993).
- <sup>9</sup>V. Tikhonchuk, *Phys. Rev. Lett.* **89**, 209301 (2002).
- <sup>10</sup>J. Yoshii, C. H. Lai, T. Katsouleas, C. Joshi, and W. B. Mori, *Phys. Rev. Lett.* **79**, 4194 (1997).
- <sup>11</sup>N. Yugami, T. Hagashiguchi, H. Gao, S. Sakai, K. Takahashi, H. Ito, Y. Nishida, and T. Katsouleas, *Phys. Rev. Lett.* **89**, 065003 (2002).
- <sup>12</sup>Z.-M. Sheng, K. Mima, and J. Zhang, *Phys. Plasmas* **12**, 123103 (2005).
- <sup>13</sup>B. Layer, A. York, and H. Milchberg, *Bull. Am. Phys. Soc.* **51**, 102 (2006); **51**, 337 (2006); and in *AIP Conf. Proc.* **877**, 750 (2006).
- <sup>14</sup>S.-Y. Chen, J. Wang, and J.-Y. Lin, *AIP Conf. Proc.* **877**, 117 (2006).
- <sup>15</sup>C. G. Durfee, III and H. M. Milchberg, *Phys. Rev. Lett.* **71**, 2409 (1993); C. G. Durfee, III, J. Lynch, and H. M. Milchberg, *Opt. Lett.* **19**, 1937 (1994).
- <sup>16</sup>T. R. Clark and H. M. Milchberg, *Phys. Rev. Lett.* **81**, 357 (1998).